ONE ELECTRON IN A CAVITY

G. GABRIELSE and J. TAN
Department of Physics, Harvard University, Cambridge, Massachusetts

I. Introduction

Measurements of the anomalous magnetic moment of the electron a provide the most stringent test of quantum electrodynamics (QED) (Kinoshita, 1990a). This theory predicts corrections to the simplest Dirac theory due to the interaction of an electron with the fluctuating radiation modes of the electromagnetic vacuum. It relates a to an asymptotic series in powers of the fine structure constant α,

$$a = c_1\left(\frac{\alpha}{\pi}\right) + c_2\left(\frac{\alpha}{\pi}\right)^2 + c_3\left(\frac{\alpha}{\pi}\right)^3 + c_4\left(\frac{\alpha}{\pi}\right)^4 + \cdots . \tag{1}$$

Over four decades, measurements of a (Conti *et al.*, 1974; Van Dyck *et al.*, 1987b; Van Dyck, 1990) and α were greatly improved, as were QED calculations[1] of the expansion coefficients c_i. The highest accuracy measurements (Van Dyck *et al.*, 1987b; Van Dyck, 1990) of a employ a

ISBN 0-12-092245-2

single electron in a Penning trap (Brown and Gabriese, 1986) to obtain an accuracy $\Delta a/a < 4 \times 10^{-9}$. The unrivaled comparision of a measured and calculated property of an elementary particle reveals an agreement $\Delta a/a < 4 \times 10^{-8}$, which would have astounded those who were struggling to formulate renormalized QED.

A few years ago, experimental progress in measuring the anomalous magnetic moment a was seriously interrupted. The electromagnetic vacuum in which the electron was located was discovered to be significantly modified by the metal electrodes of the Penning trap (Gabrielse and Dehmelt, 1985) represented in Fig. 1. Electron cyclotron motion around a vertical magnetic field $B = 6$ Tesla is at frequency[2]

$$\omega_c = \frac{eB}{mc} = 2\pi(164\ \text{GHz}). \tag{2}$$

Cyclotron motion in free space would damp via synchrotron radiation at

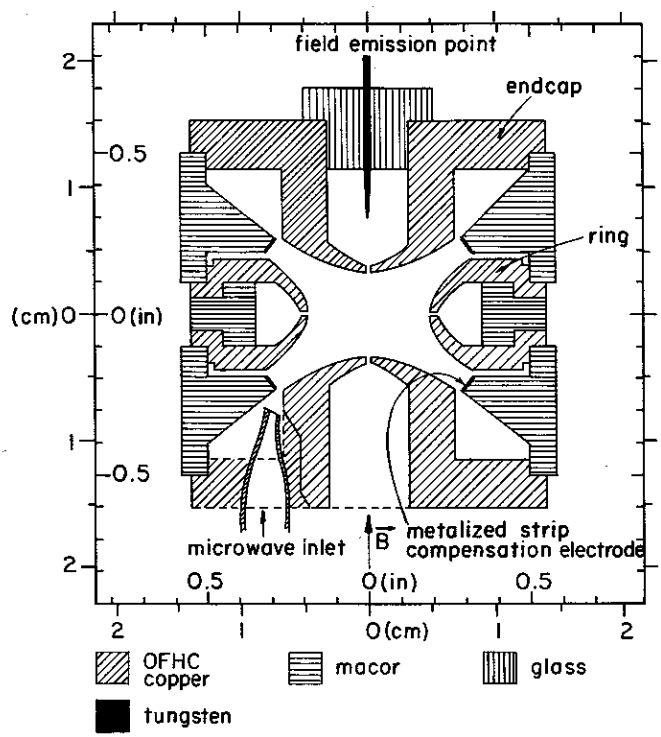

FIG. 1. Hyperbolic Penning trap in which the inhibited spontaneous emission of a one-electron cyclotron oscillator was first observed. (From Gabrielse and Dehmelt, 1985.)

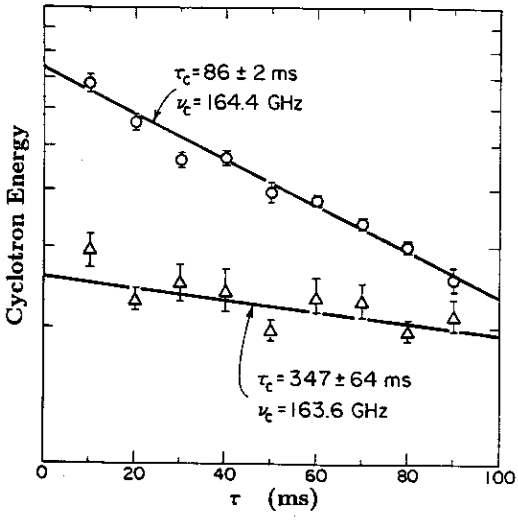

FIG. 2. Measured energy decay of a one-electron cyclotron oscillator in the hyperbolic trap as a function of time for two cyclotron frequencies. Spontaneous emission is clearly inhibited in both examples compared with the decay rate of 75 ms in free space. (From Gabrielse and Dehmelt, 1985.)

a rate

$$\gamma_c = \frac{4e^2\omega_c^2}{3mc^2} = (0.1\ \mathrm{s})^{-1} \tag{3}$$

Instead, Fig. 2 shows an observed decay of cyclotron energy (Gabrielse and Dehmelt, 1985) for a single electron in the trap, which is decidedly less by a factor of 3, the first observation of inhibited spontaneous emission within a microwave cavity.[3] Corresponding cavity shifts of measured frequencies, calculated (Brown *et al.*, 1985a,b, 1988) but not yet observed, were estimated to be the largest experimental uncertainty (Van Dyck *et al.*, 1987b; Van Dyck, 1990) based upon the calculations. To complicate this serious problem, so little was known about the radiation field within trap cavities that the uncertainty estimate is itself rather suspect. Also, the traditional hyperbolic electrode geometries such as those shown in Fig. 1 do not allow easy calculation (Brown *et al.*, 1988) or even a ready classification of the standing-wave fields in cavity radiation modes. Even if mode eigenfrequencies were known, the field configuration and hence the coupling of a centered electron to any particular cavity mode (if any) would not be known.

New experiments (Tan and Gabrielse, 1991, 1993) show how to change

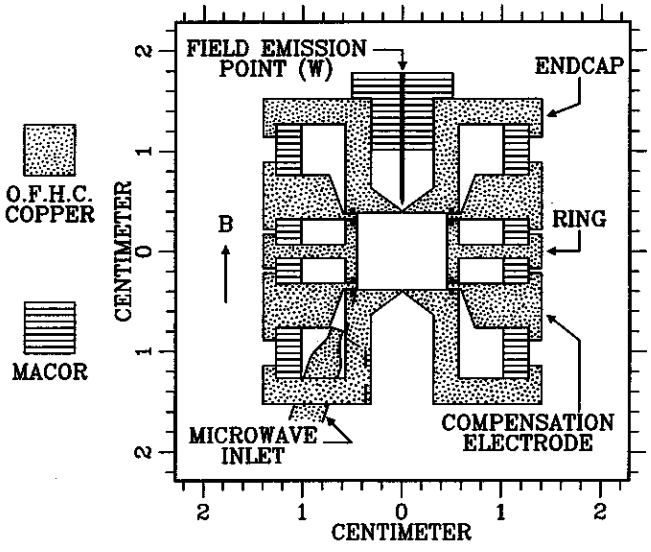

FIG. 3. An orthogonalized cylindrical trap cavity has a spatially uniform magnetic field along the vertical axis.

the cavity-modified vacuum from a serious interruption into an advantage. The key (Section II) is a trap (Fig. 3) that is a good approximation to an ideal cylindrical cavity (Fig. 4). Geometrical tricks (Gabrielse and MacKintosh, 1984) allowed us to obtain an electrostatic quadrupole potential of sufficient quality to observe a single trapped electron (Tan

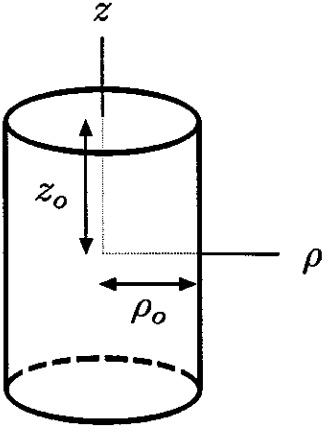

FIG. 4. Ideal cylindrical cavity.

and Gabrielse, 1989) with a signal-to-noise ratio as good as in the hyperbolic traps used earlier. A new technique, with parametrically pumped electron oscillators, allows the frequencies and quality factors for radiation modes of a trap cavity to be cleanly observed and measured for the first time. Frequencies of more than 100 observed modes below 166 GHz correspond to those of an ideal cavity to typically 1% or better. This makes it possible to identify the standing-wave fields using familiar classifications (Jackson, 1975) (e.g., TE_{115}). Some of these field configurations couple to an electron's cyclotron motion at the trap center. Others should allow rapid change of cyclotron damping (Section III.B), sideband cooling of an electron to very low (mK) temperatures (Section III.C), and directly driven spin flips. The cavity-modified vacuum is an advantage insofar as measured linewidths are narrowed when the electron cyclotron oscillator radiates less than in free space. This is arranged by tuning the magnetic field so that the electron cyclotron frequency is not resonant with the resonant frequency of a cavity mode that couples to the electron. Simple theory yields damping rates (e.g., Fig. 5a) and frequency shifts (e.g., Fig. 5b), which can be experimentally confirmed and used to avoid attendant frequency shifts, making possible a new generation of measurements of the electron magnetic moment (Section III.A). The simple

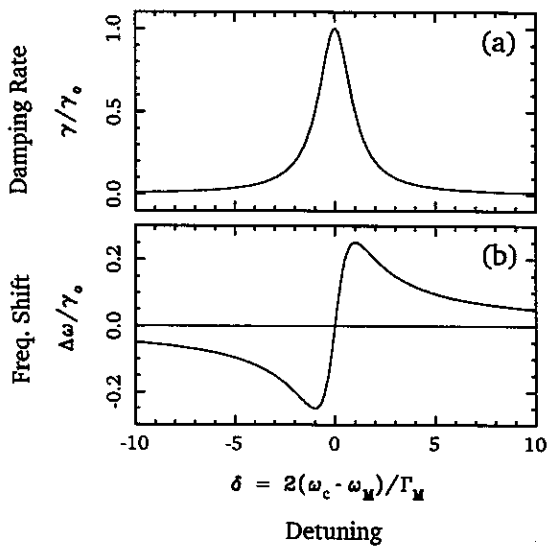

FIG. 5. Characteristic dependence of an oscillator's damping rate γ (a) and frequency shift $\Delta\omega$ (b), as a function of its detuning δ from the resonant frequency of a coupled cavity mode (or LCr circuit).

theory of the interaction between an electron oscillator and a single mode of the radiation field is summarized in Section IV.

Although the importance of cavity shifts for measurements of the electron magnetic moment was demonstrated only recently, the basic notion that the couplings of two oscillators can shift both the damping rate and oscillation frequency of the oscillations is certainly very familiar. (The electron cyclotron motion and an electromagnetic cavity mode are the coupled oscillators here.) Long ago, for example, it was mentioned that the spontaneous emission of an atom placed in a cavity could be inhibited (Purcell, 1946). Further discussions of cavity-induced modifications to atom damping rates came later (Kleppner, 1981), with clear realization of the problems that the frequency shifts would present for precise measurements of resonance frequencies (Kleppner, 1971). In fact, soon after the observation of inhibited spontaneous emission in a trap cavity, similar effects were observed with Rydberg atoms traveling between parallel conducting plates (Hulet *et al.*, 1985) and in another Penning trap (Van Dyck *et al.*, 1987b; Van Dyck, 1990). Related studies with Rydberg atoms continue.[4,5] Some additional evidence for the presence of cavity modes in a hyperbolic trap has also been observed (Van Dyck *et al.*, 1987a), but it remains difficult to interpret since signal-to-noise ratio was poor, no Lorentzian lineshapes were established, and no information about the standing-wave field configuratons (and hence the coupling to a trapped electron) could be deduced.

The well-characterized, standing-wave fields of the cylindrical trap cavity revive interest in cavity shifts of an electron's spin precession frequency. Theoretical studies first suggested that the cavity-modified vacuum could be responsible for shifts large enough to be observable (Fishbach and Nakagawa, 1984a). Boulware and Brown (1985) contradicted the initial claim. Many other theoretical papers are written (Fishbach and Nakagawa, 1984b; Boulware *et al.*, 1985; Svozil, 1985; Kreuzer and Svozil, 1986; Tang, 1987; Kreuzer, 1988; Barut and Dowling, 1989). The latest work seems to support the contradiction of the initial claims, even though opposing conclusions have never been resolved as completely as might be desired. The theoretical studies share the common difficulty of making a calculable model (e.g., a spin near a conducting plate or plates) that is also a reasonable approximation to an electron in a trap cavity. It remains to study theoretically the resonant interaction of a spin with one of the high Q modes of the cylindrical trap cavity that couple most strongly to a spin. If it is experimentally demonstrated that cavity shifts of the cyclotron frequency are well understood (Section III.A), cavity shifts of the spin frequency could then be investigated experimentally as well.

II. Cylindrical Penning Trap Cavity

A. Ideal Cylindrical Cavity

In the following sections we show how it is possible to suspend a single electron near the center of a Penning trap cavity that closely approximates an ideal cylindrical cavity of height $2z_0$ and radius ρ_0 (Fig. 4). The goal is precise understanding and control of the electron–cavity interaction, and this requires well-characterized standing-wave fields within which the electron can be localized. Traditional hyperbolic Penning traps formed cavities for which it has not yet been possible to even classify the standing-wave fields. In marked contrast, the radiation modes of a simple cylindrical cavity are classified in a familiar way as either transverse magnetic or transverse electric modes. The eigenfrequencies ν_{mnp} are given by (Jackson, 1975)

$$2\pi\nu_{mnp} = c\sqrt{\left(\frac{\chi_{mn}}{\rho_0}\right)^2 + \left(\frac{p\pi}{2z_0}\right)^2}, \tag{4}$$

where c is the speed of light. For transverse magnetic modes TM_{mnp}, the χ_{mn} is the nth zero of the mth order Bessel function $J_m(x)$ and $p = 0, 1, 2, \ldots$. For transverse electric modes TE_{mnp}, the χ_{mn} is the nth zero of the Bessel function derivative $J'_m(x)$ and $p = 1, 2, \ldots$. In both cases, $m = 0, 1, \ldots$ and $n = 1, 2, \ldots$.

The electromagnetic fields for each of the standing-wave modes are simple analytic functions (Jackson, 1975). This makes it straightforward to calculate the interaction of particlar cavity radiation modes with a single electron localized in the trap cavity. Of particular interest are the standing-wave modes that couple to electron cyclotron motion, which is perpendicular to the axis of the cylinder and typically near to it. Such coupling requires an electric field perpendicular to the cylinder axis. This is provided by either TE_{1np} or TM_{1np} standing-wave modes, provided that the electron is not localized in an axial standing wave minimum. For example, the transverse electric fields of TE_{1np} modes near the symmetry axis of the cavity are simple sine and cosine functions of the z coordinate (relative to the center of the cavity). The quantum number p indicates the number of standing-wave maxima (antinodes) that fit between the two endcaps. For modes with odd p, components of the transverse electric field,

$$E_\perp = E_0 \cos\left(\frac{\pi p z}{2z_0}\right) e^{-i\omega t}, \tag{5}$$

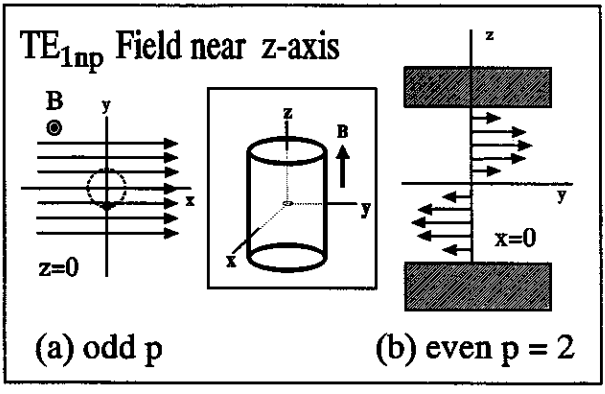

FIG. 6. Representation of the transverse electric field for TE_{1np} modes: (a) in the midplane for odd p and (b) along the z axis for even p.

have a maximum in the midplane as illustrated in Fig. 6(a). These odd p modes, with their electric field maxima near the trap center, couple strongly to electron cyclotron motion at the center of the trap. These modes are thus particularly suited for driving a centered cyclotron oscillator with an external microwave source. They provide efficient damping of electron cyclotron motion as well, but they also cause associated frequency shifts, as we shall see. For the related modes with p even, the electric field vanishes in the midplane (Fig. 6b)

$$E_{\perp} = E_0 \sin\left(\frac{\pi p z}{2z_0}\right) e^{-i\omega t}. \tag{6}$$

The even p modes thus do not couple to the cyclotron motion of an electron at the center of the cavity. Spatially displacing the electron from node to antinode, however, provides a way to rapidly couple and uncouple the electron and cavity, turning the cyclotron damping from on to off (Section III.B). Moreover, the spatial gradients near the nodes are suited for sideband cooling thermal motions of the electron along the cavity axis (Section III.C).

B. Observing a Single Electron

Electrons can be suspended and studied within a cavity if the cavity walls are split to allow them also to serve as the electrodes of a Penning trap. A single electron can be suspended and studied if, in addition, the potential produced by voltages applied to the trap electrodes is a high quality

electrostatic quadrupole. This results in harmonic oscillations of the trapped particles at a well-defined and precisely measurable frequency. Traditionally, such a quadrupole potential was produced using metal electrodes painstakingly shaped along the hyperbolic equipotentials of the desired electrostatic quadrupole. The Penning trap used to observe inhibited spontaneous emission for the first time (Fig. 1) is one example. A single electron was stored 10 months in this hyperbolic trap and was used to observe the relativistic hysteresis and bistability of a single electron at extremely low, meV energies (Gabrielse *et al.*, 1985), illustrating the sensitivity that is relevant.

In more detail, the desired electrostatic quadrupole potential can be written as

$$V = V_0 \frac{z^2 - \rho^2/2}{2d^2} C_2, \tag{7}$$

where V_0 is the potential applied to the electrodes, d is an appropriate trap dimension, and C_2 is a dimensionless constant that depends upon the electrode geometry. The axial dimension z is the distance from the center of the trap along the magnetic field direction, and ρ is the corresponding radial coordinate. A trapped particle of charge q and mass m oscillates harmonically in this potential, along the magnetic field direction, at axial frequency ω_z given by

$$\omega_z^2 = \frac{qV_0}{md^2} C_2. \tag{8}$$

Typically, the axial oscillation frequency is monitored precisely, with small shifts in this frequency used to derive information about the cyclotron motion of the trapped electron. For a harmonic oscillation, small amplitude fluctuations do not change the oscillation frequency. A single trapped electron can be observed and studied precisely when it oscillates harmonically, when the additions to the electrostatic quadrupole are small.

To approximate an ideal cylindrical cavity, the trap cavity in Fig. 3 was precisely constructed with small slits (0.015 cm) that incorporate choke flanges ($\lambda/4$ at 164 GHz). Although this cylindrical geometry is a greatly improved way to understand and control the radiation field in the trap cavity, it is a much less straightforward way to produce the high quality electrostatic quadrupole potential. The trap cavity has its vertical axis $\hat{z}$ along the axis of a 6 Telsa magnetic field from a superconducting solenoid. Small slits perpendicular to the magnetic field divide the oxygen-free high-conductivity copper cavity walls into two endcap electrodes (at z_0 above and below the trap center), a ring electrode (with

radius ρ_0), and two compensation electrodes. A judicious choice of the ratio ρ_0/z_0 yields a crucial orthogonalization property (Gabrielse and MacKintosh, 1984). Leading deviations that are unavoidably added to the desired electrostatic quadrupole potential in Eq. (7),

$$\Delta V = \frac{1}{2} C_4 V_0 \frac{z^4 - 3z^3\rho^2 + \frac{3}{8}\rho^4}{d^4} + \frac{1}{2} C_6 V_0 \frac{z^6 - \frac{15}{2}z^4\rho^2 + \frac{45}{8}z^2\rho^4 - \frac{5}{16}\rho^6}{d^6}, \tag{9}$$

can be tuned (by adjusting potentials on the compensation electrodes) so that $|C_4| < 10^{-5}$ and $C_6 \approx -10^{-1}$, with negligible change in the strength $C_2 V_0$ of the desired electrostatic quadrupole. The axial oscillation of a single electron can thus be observed at a fixed axial oscillation frequency ω_z while the trap is tuned to make the oscillation more harmonic.

Once the potential is tuned, the motions of a trapped electron in a cylindrical trap are the same as in a hyperbolic trap. The three familiar motions (Brown and Gabrielse, 1986) include a cyclotron orbit around magnetic-field lines (at frequency $\omega_c'/2\pi < 170$ GHz), a harmonic axial oscillation along the magnetic field direction $\hat{z}$ (at frequency $\omega_z/2\pi = 63$ MHz), and a circular magnetron motion (at a much lower frequency $\omega_m = 12$ kHz), which is not important for the cavity electrodynamics. The cyclotron frequency in the trap ω_c' is shifted slightly from the cyclotron frequency ω_c for an electron in a magnetic field alone, but this difference is also not important for these studies. Figure 7 shows a driven axial resonance for a single trapped electron that is less than 4 Hz wide. With this signal-to-noise ratio, a shift in the axial resonance frequency of

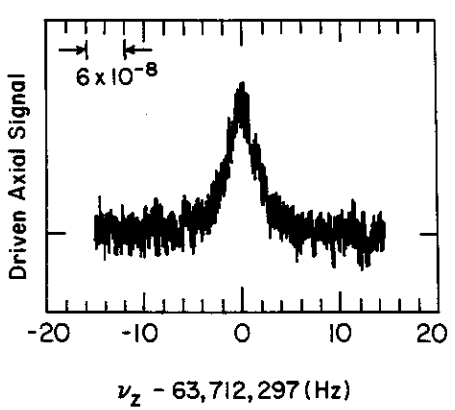

FIG. 7. Driven axial resonance of one electron in a cylindrical Penning trap.

1 Hz out of 64 MHz is easily resolved, a resolution that is as good as has been obtained in hyperbolic traps.

C. Observing Cavity Radiation Modes 0–166 GHz

Despite great attention to making a cylindrical Penning trap cavity that is a good approximation to an ideal cylindrical cavity, the small slits, holes, and uncontrolled imperfections unavoidably shift the radiation eigenfrequencies of the trap cavity from those of an ideal cylindrical cavity. The hope is that the shifts are small, so that measured eigenfrequencies can still be used to identify the modes. Furthermore, small shifts would indicate that the standing-wave fields in the trap cavity are essentially the simple analytic forms already discussed.

A technique using synchronized electrons in the trap (Tan and Gabrielse, 1991, 1993) allows us to observe the actual modes of the trap cavity in situ, after the electrodes have contracted from being cooled to 4 K. A simplified model of the detection system is depicted in Fig. 8. The parametrically excited electron oscillators (modeled in Fig. 8 by massive balls attached to springs) are bound near the midplane of the trap cavity (represented by the parallel-plate conductors). The restoring force of the springs is modulated with strength h and at frequency ω_d, and hence the axial oscillators have spring "constants"

$$m\omega_z^2[1 + h\cos(\omega_d t)]. \tag{10}$$

The oscillatory motions of the electrons induce a current through the resistor connected between the two plates (representing the endcaps of the trap cavity). The voltage drop across this resistor is amplified, squared, and filtered to give a signal that is proportional to the energy in the axial center-of-mass (CM) motion. Under appropriate conditions this signal is coherent with the drive, a manifestation of interesting nonlinear dynamics and cooperative behavior that is discussed in Tan and Gabrielse, 1991, 1993, but is outside the scope of this chapter.

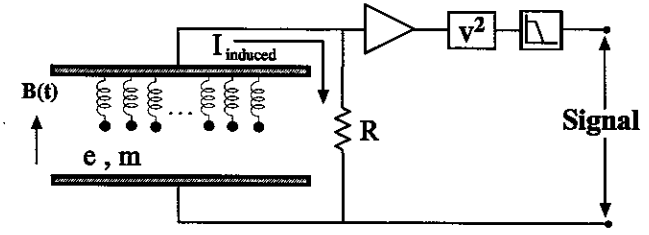

FIG. 8. Simplified model of parametrically excited electron oscillators and detection electronics.

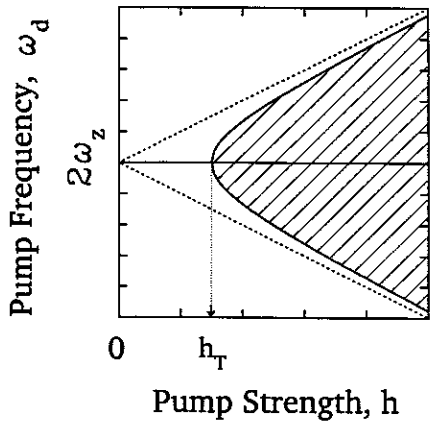

FIG. 9. Drive frequency versus strength for the parametric pump showing the region of Mathieu instability (cross-hatched).

To probe the microwave cavity modes, it suffices to observe that there is a well-defined region in the parameter space (h, ω_d) of the parametric pump wherein the signal is sensitive to radiative cooling by the trap cavity. This region is cross-hatched in Fig. 9. Figure 10(b) shows the measured frequency response with the pump strength held fixed at a value above the threshold. This family of superimposed resonances is obtained by varying the detuning between the cavity-mode frequency

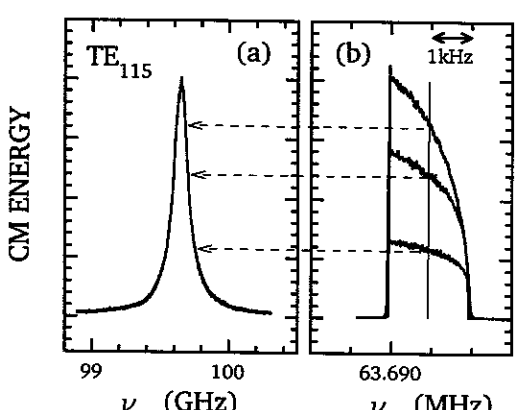

FIG. 10. (a) Cavity resonance observed by monitoring the axial center-of-mass energy while driving parametrically at $\omega_d = 2\omega_z$. The magnetic field is swept slowly in time to vary ω_c'. (b) Parametric axial resonances for indicated detunings of the cylcotron and cavity mode frequencies. The electrons are cooled less efficiently as this detuning is increased.

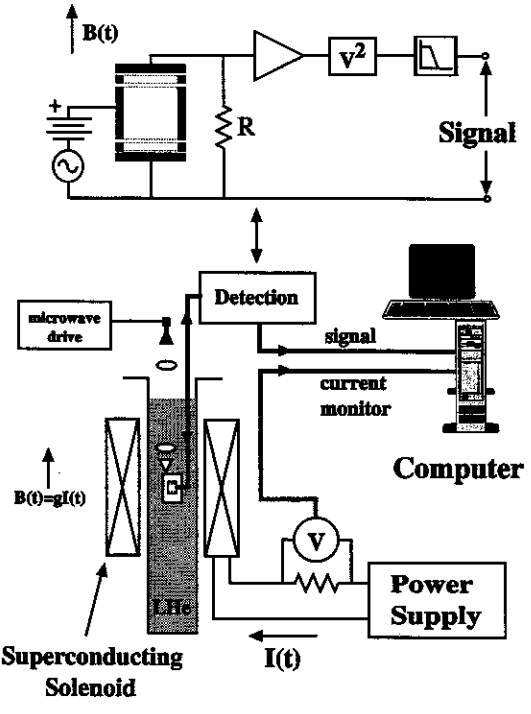

FIG. 11. Simplified diagram of the experimental apparatus for cavity-mode detection.

and the electron cyclotron frequency. It clearly shows that the signal grows with increasing radiative cooling and reaches a maximum when the cyclotron frequency is swept into resonance with the cavity mode. Cavity modes are thus conveniently detected by fixing the pump frequency at $\omega_d = 2\omega_z$ and monitoring the axial CM energy, while the cyclotron frequency is being swept, as illustrated in Fig. 10(a).

A simplified overview of the apparatus is shown in Fig. 11. The trap is sealed in a high-vacuum envelope, which is cryopumped via thermal contact with a liquid helium bath. The magnetic field is generated by a superconducting solenoid designed for precise studies with nuclear magnetic resonance. Since the cyclotron frequency is proportional to the magnetic field, we sweep the current in the superconducting solenoid up to 5.9 Tesla (slowly, because the solenoid inductance is 200 Henries) in order to tune the cyclotron oscillators into resonance with one cavity mode after another. A measure of the current in the solenoid and the signal from the electron oscillators are digitized simultaneously and stored in a computer. (A conversion from measured solenoid current to

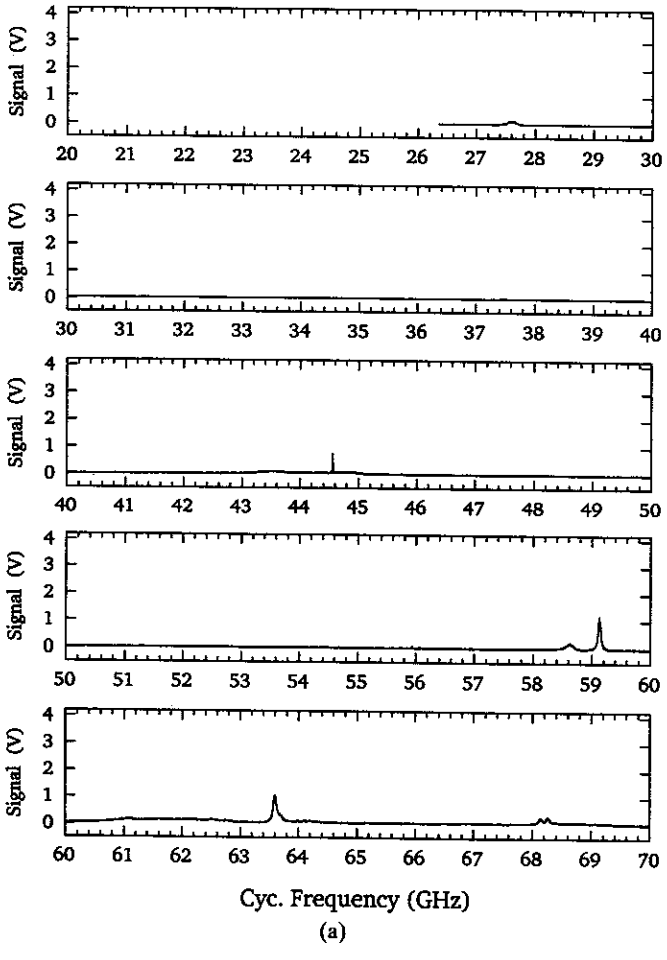

FIG. 12. Observed cavity modes below 166 GHz.

cyclotron frequency is obtained by exciting an electron cyclotron resonance with a microwave source.) A full spectrum for 0 to 166 GHz is shown in Fig. 12 and takes about 10 hours to obtain. The extraordinary sensitivity of the synchronized motion of the electron oscillators to radiative cooling via energy transfer to the modes of the trap cavity allows us to observe even weakly coupled cavity modes (e.g., those with nodes in the midplane), presumably because the electrons occupy a volume extending slightly away from the center of the trap. Isolated resonances have Lorentzian lineshapes, as illustrated by the data points

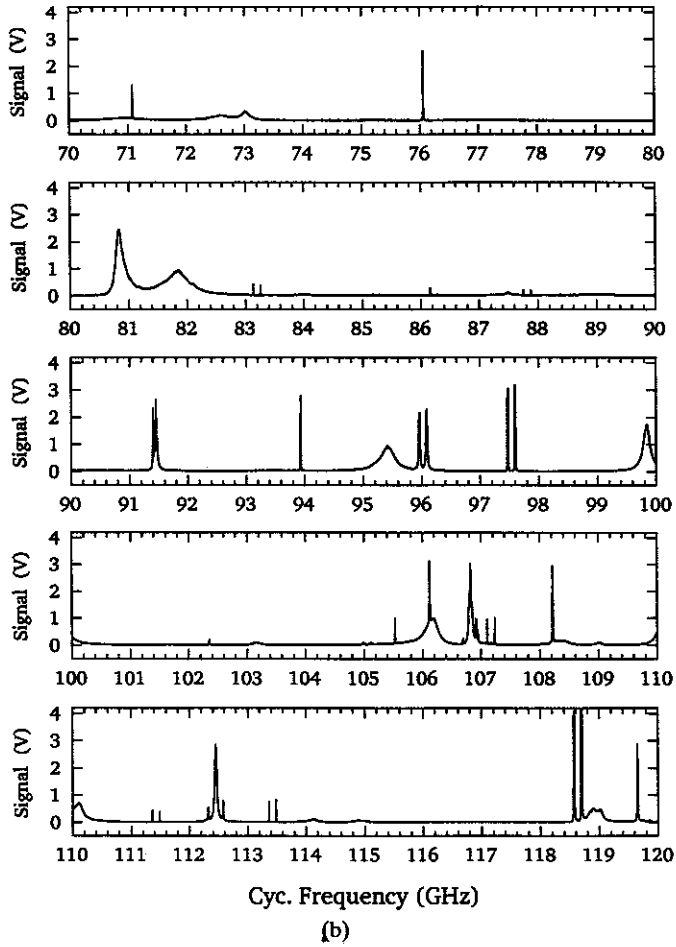

FIG. 12—(*Contd.*)

and Lorentzian fits for the two modes in Fig. 13. Thermal cycling of the trap apparatus up to 300 K and back to 4.2 K changes the observed resonance frequencies by less than 0.1%.

The TE_{0np} modes are unusual in that these azimuthally symmetric modes are singlets, unlike $m > 0$ modes, which are doubly degenerate. In the observed spectrum, however, TE_{0np} resonances with even p appear near the frequencies expected for an ideal cylinder in Eq. (4), but they appear as doublets. Modes with p even have a node in the midplane of the trap and are thus decoupled from the cyclotron motion of electrons located exactly at the center of the trap. The periodic axial motion of the

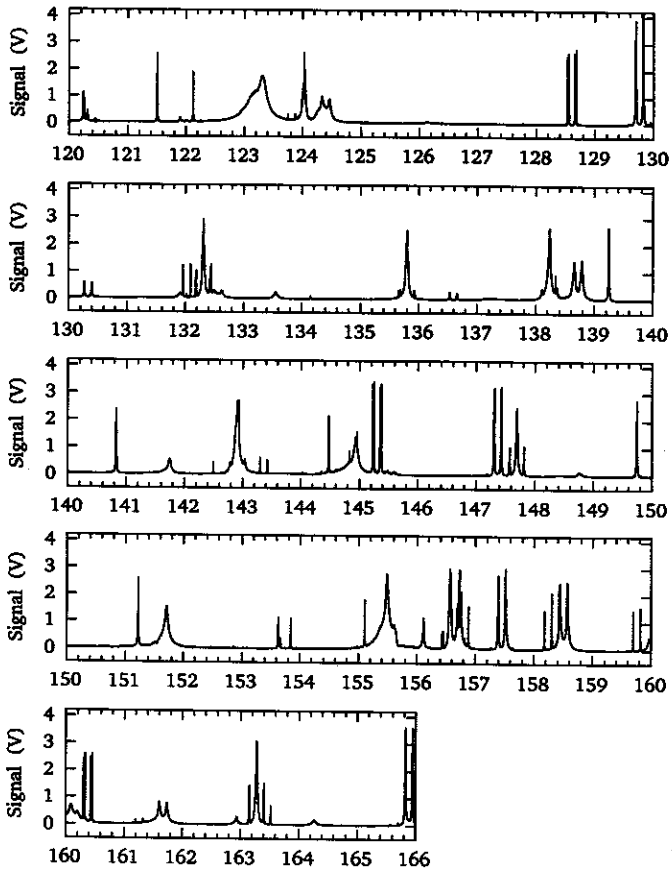

(c)

FIG. 12—(*Contd.*)

electrons, driven by the parametric pump, makes the electrons sample the standing-wave field away from the node at the center of the trap. The microwave field experienced by the oscillating electrons is thus amplitude modulated, which produces the observed sidebands. Plotting the frequency separations for the doublets (Fig. 14) shows clearly that the splittings are twice the axial oscillation frequency, as would be expected. All even p modes, regardless of m value, give similar motional splitting in the spectrum, as illustrated in Fig. 15(a). The motional effect is different (and typically smaller) for odd p modes, since these have a maximum of the standing-wave field at the center of the trap. Nevertheless, for

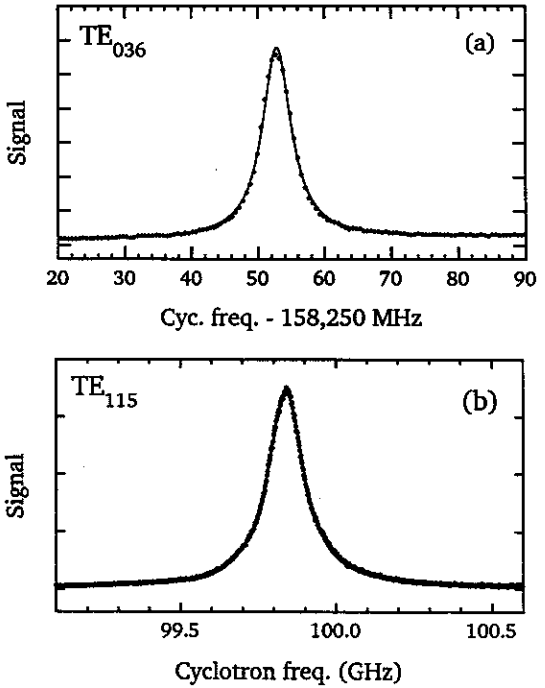

FIG. 13. Lorentzian lineshapes fit to observed cavity modes that are well separated from other modes.

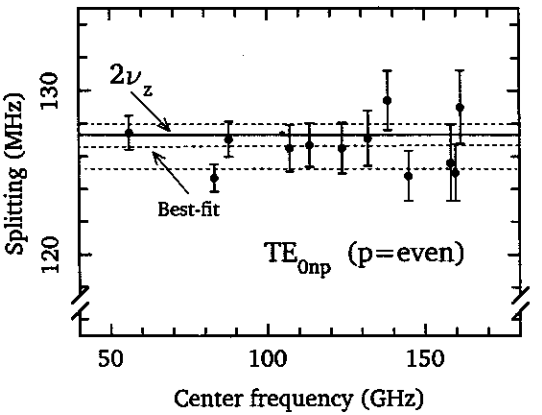

FIG. 14. Motional splitting of singlet modes TE_{0np}. The best fit (center dashed line) is consistent with $2\nu_z$ (solid line) within its uncertainty (dashed lines above and below).

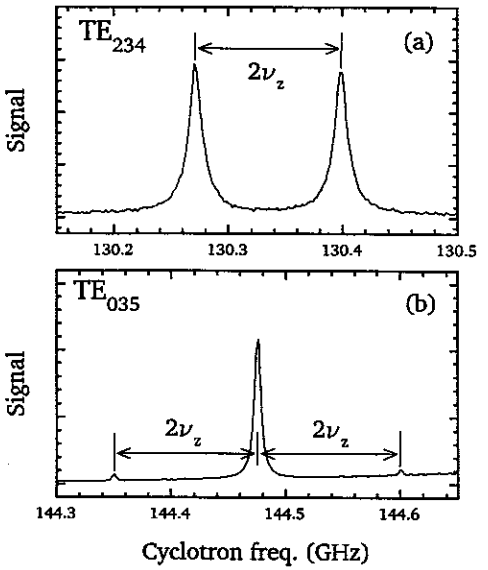

FIG. 15. (a) Motional doublet for a mode with p even has separation of $2\nu_z$. (b) Motional sidebands for a mode with odd p are separated from the strong central peak by $2\nu_z$.

sufficiently large oscillations and for large p, small sidebands are observed at $2\nu_z$ to either side of the strong central peak as illustrated in Fig. 15(b).

With motional sidebands understood, the measured frequencies correspond well to those for a perfect cylindrical cavity, offering the possibility of identifying resonant modes of a trap cavity for the first time. The azimuthally symmetric TE modes with $m = 0$ have high Q values and are not shifted much by the slits because induced surface currents flow parallel to the slits, allowing the effective trap dimensions to be determined in situ at 4 K to within 6 μm, as shown in Fig. 16. A best fit of Eq. (4) to 12 measured eigenfrequencies for such modes yields a rms frequency deviation of 0.08% and dimensions $\rho_0 = 0.4559(6)$ cm and $z_0 = 0.3838(6)$ cm, in good agreement with our expectations based upon machining tolerances and expected thermal contraction. Taking the observed width at half maximum divided by the resonant frequency to be Q^{-1}, the mean Q is 20,000 with an rms spread of 6500.

For other field symmetries of experimental interst, Fig. 17 shows percentage deviations of measured and calculated resonant frequencies. There is good agreement. The most important modes (Brown *et al.*, 1985b; Brown and Gabrielse, 1986; Gabrielse *et al.*, 1990), those with p

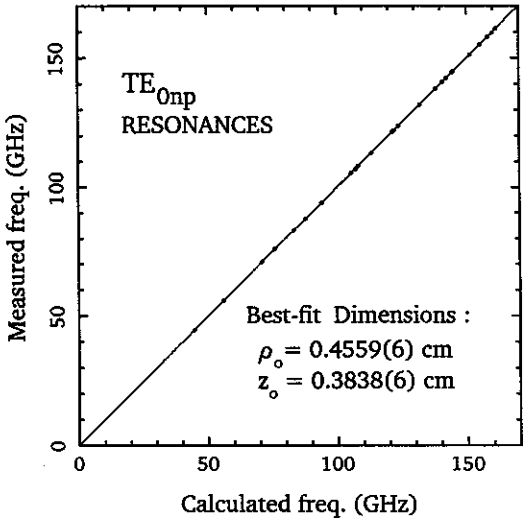

FIG. 16. The fit of measured TE_{0np} mode eigenfrequencies to those calculated for an ideal cylinder in Eq. (4), in situ at 4 K, determines effective dimensions of the trap cavity to within 6 μm.

odd and $m = 1$, have nonvanishing transverse electric fields at the cavity center and hence couple directly to the small cyclotron orbit of an electron. The strong coupling results in the largest observed resonance signals (i.e., largest peak area in Fig. 12) for the 29 of these modes that we observe. Frequency deviations are typically 1%, which is larger than for the TE_{0np} modes in the foregoing, as expected. Nonetheless, the shifts are still typically five times smaller than the average mode spacing, though mode overlap gets more likely as the mode density increases at higher frequencies. The mean Q is 1300, with a spread of 1100 and a highest Q of 3700.

Isolated modes fit well to Lorentzian lineshapes, as has been illustrated, with exceptions in two interesting cases. First, for modes with standing-wave nodes in the midplane of the trap, the axial oscillation in the linear gradient near the node plane causes motional sidebands as discussed. The second exception is the modification of the lineshape when an electron cloud and a cavity mode are strongly coupled. The coupling increases in proportion to the square of the number of electrons N and in proportion to Q. When N and Q are sufficiently large, the coupling time for the cloud and mode is therefore shorter than the decay time for the cavity mode itself. To illustrate the lineshape modification, Fig. 18(a) shows the observed resonance for TE_{115}, which fits well to a Lorentzian

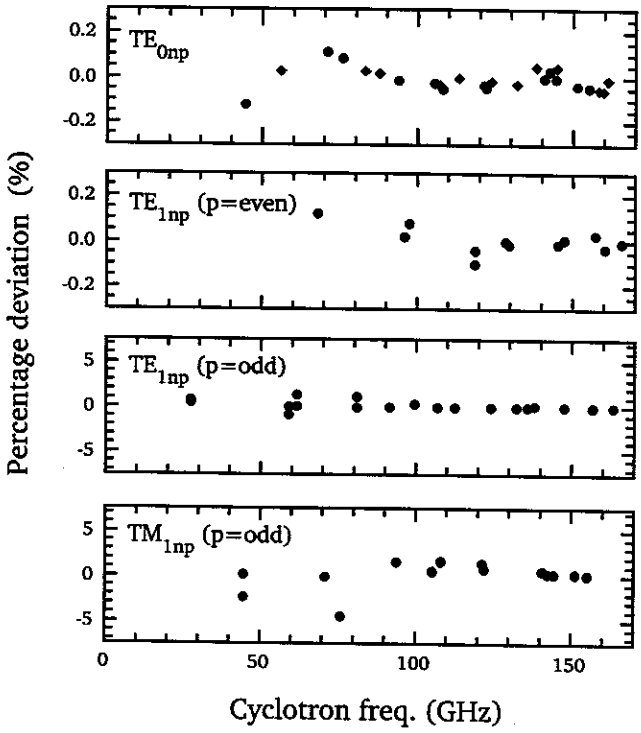

FIG. 17. Comparison of observed and calculated eigenfrequencies for series of cavity modes of particular experimental interest.

lineshape, with a small number of electrons. The number of electrons is increased in Fig. 18(b), resulting in broadening of the line, especially at its base. With further increase in trapped electrons, the observed resonance is split, as shown in Fig. 18(c).

III. New Generation of Electron Measurements

A. Magnetic Moments Without Cavity Shifts

Cavity shifts presently limit the precision of the measured magnetic moments of the electron and positron, as we have seen. Inhibited spontaneous emission in the cyclotron motion has been observed in these experiments, with cyclotron decay time longer than in free space. The

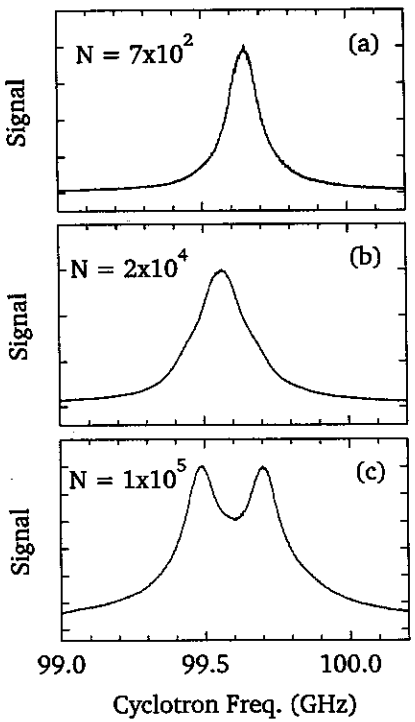

FIG. 18. The Lorentzian lineshape (a) is modified to the strongly coupled lineshapes in (b) and (c) as the number of electrons N is increased to increase the electron–cavity coupling.

corresponding frequency shift that must be present (illustrated in Fig. 5b), however, has not been determined because the microwave properties of the hyperbolic trap are virtually unknown experimentally and are difficult to deal with even in principle. Consequently, the latest measurements of the magnetic moment for the electron and positron,

$$a(e^-) = 0.001\,159\,652\,188\,4\,(14)\,(40), \tag{11}$$

$$a(e^+) = 0.001\,159\,652\,187\,9\,(14)\,(44), \tag{12}$$

are reported with the largest uncertainty (40) due to cavity shifts (Van Dyck *et al.*, 1987b; Van Dyck, 1990). This uncertainty, considered as the "most probable" cavity shift in the cyclotron frequency, was crudely estimated using our calculations for a cylindrical cavity model, which is not a very satisfying approximation to a hyperbolic trap cavity.

QED calculations of the electron's anomalous magnetic moment have

been pushed to nearly the same accuracy (Kinoshita, 1990b). As mentioned earlier, however, QED relates measured a values to measured values of the fine structure constant α. For comparision with the measured a values, the QED calculation and the measured fine structure constant together give an anomalous magnetic moment

$$a = 0.001\,159\,652\,140\,0\,(53)\,(41)\,(271). \tag{13}$$

The uncertainties of (53) and (41) come from numerical calculations of the expansion coefficients c_3 and c_4 in Eq. (1), respectively. The largest uncertainty (271) comes from uncertainty in the fine structure constant as measured using the quantum Hall effect. In the future, it may be possible to determine α more accurately using (Taylor, 1991)

$$\alpha^2 = \frac{2R_\infty}{c}\frac{M(\mathrm{Na})}{M_\mathrm{p}}\frac{M_\mathrm{p}}{m_\mathrm{e}}\frac{h}{M(\mathrm{Na})}, \tag{14}$$

provided that $h/M(\mathrm{Na})$ can be measured accurately using atom interferometry as is hoped (Kasevich and Chu, 1991). The latest adjustment of fundamental constants is based in part on a somewhat more precise determination of α obtained by combining the QED calculation (assuming the exact validity of QED) with the measurement of a to obtain

$$\alpha^{-1}(\mathrm{QED}) = 137.035\,992\,22\,(94). \tag{15}$$

The uncertainty in this QED determination of the fine structure constant is 7×10^{-9} if the shift estimate turns out to be accurate.

Controlling the interaction of an electron cyclotron oscillator with the cavity-modified vacuum will be crucial for higher precision tests of QED. Better a measurements in trap cavities of unknown microwave properties appear difficult and unlikely. For example, using lossy materials and electrodes would make a hyperbolic trap cavity approximate the free-space vacuum (and thus avoid shifts due to unknown standing-wave fields). The cyclotron damping width would also be as large as in free space, however, making precise frequency measurements more difficult. To relate the uncertainty $\Delta\omega_\mathrm{c}$ in measuring the cyclotron frequency to the resulting uncertainty Δa in the measured anomalous magnetic moment a, we note that

$$a = \frac{\omega_\mathrm{s} - \omega_\mathrm{c}}{\omega_\mathrm{c}} \tag{16}$$

can be regarded as a definition of a, where ω_s is the electron's spin

precession frequency. Since $a \approx 10^{-3}$ is small,

$$\frac{\Delta a}{a} \approx \frac{1}{a}\frac{\Delta\omega_c}{\omega_c}. \tag{17}$$

For $B = 5.9$ Telsa, without line splitting, the cyclotron frequency could therefore (in principle) be measured to 8×10^{-12}, from Eqs. (2) and (3) in (16). Setting $\Delta\omega_c$ equal to the free-space linewidth yields $\Delta a/a \approx 8 \times 10^{-9}$. The experimental error currently quoted (Van Dyck *et al.*, 1987b; Van Dyck, 1990) is already much smaller.

The cylindrical cavity, with identified p odd, $m = 1$ modes, is a greatly improved environment for experiments with a centered, one-electron cyclotron oscillator. To illustrate this point, a 10-GHz span of experimental interest is displayed in Fig. 19. Of the modes in this span, only TM_{123} and TE_{115} couple to the cyclotron motion of one electron at the center of the trap. TE_{124} and TE_{132} do not couple to one centered electron but are suited for sideband cooling of the axial motion (Section III.C). Both the damping rate γ for an electron's cyclotron motion (for small enough damping—Grabrielse and Dehmelt, 1985) and the cavity shift of its frequency $\Delta\nu$ could be measured as a function of ν_c' with one trapped electron, but this would take a very long time. To a good approximation (Gabrielse *et al.*, 1990), however, coupling to the Mth of these cavity modes (with resonant frequency ν_M) yields the explicit forms

$$\gamma = A_M \frac{Q_M}{1 + (Q_M \delta_M)^2}, \tag{18}$$

$$2\pi\,\Delta\nu = \frac{1}{2} A_M \frac{(Q_M)^2 \delta_M}{1 + (Q_M \delta_M)^2} = \frac{1}{2}\gamma Q_M \delta_M. \tag{19}$$

The constants A_M are precisely known (equivalent to those tabulated (Gabrielse *et al.*, 1990) as elaborated in Section IV) because the field configurations of these modes are known. Both γ and $\Delta\nu$ are functions of the "detuning" $\delta_M = 2(\nu_c' - \nu_M)/\nu_M$ (which is accurately controlled and measured) and the quality factor for the mode Q_M. These explicit forms, with ν_M and Q_M from the measurements described earlier (summing over nearby modes as necessary and including manageable renormalization corrections neglected here (Gabrielse *et al.*, 1990)) can be used to compute the frequency shift (Fig. 19b) and damping rate (Fig. 19c) for a centered electron. The hope is to compare these with several specific measurements with one electron and then to deduce the cyclotron frequency (i.e., the magnetic field) at which the electron's cyclotron frequency is not shifted by the cavity. The damping width is 50 times

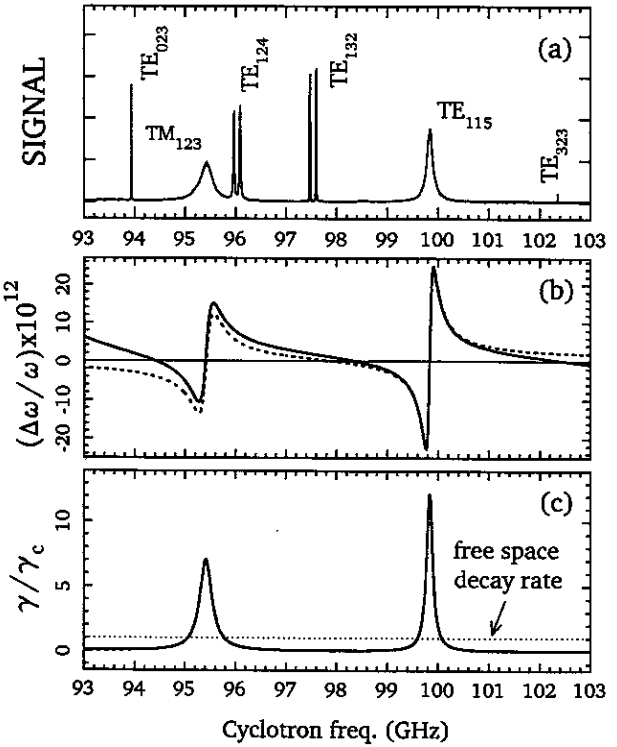

FIG. 19. Observed cavity modes in a 10-GHz spectrum (a). Corresponding frequency shifts (b) and damping rates (c) for one electron at the center of the cavity are calculated using measured Q values and resonant frequencies along with calculated coupling constants. The dashed line in (b) includes only the effect of TM_{123} and TE_{115}, which are the modes in the figure that couple to the cyclotron motion of a centered electron. The solid line also includes the effect of nearby coupled modes not in this span.

narrower than in free space at this unshifted cyclotron frequency. The likelihood for thereby improving the measurement accuracy is very high.

B. Rapid Control of Electron–Cavity Coupling

The simple standing-wave pattern of $m = 1$ modes can be used to change the cyclotron damping rate rapidly without changing the magnetic field (which would take months to restabilize sufficiently for high precision experiments). This is possible because the coupling between the cyclotron oscillator and a cavity mode vanishes at a node of the standing wave. An electron can be moved up and down by adding an antisymmetric electric

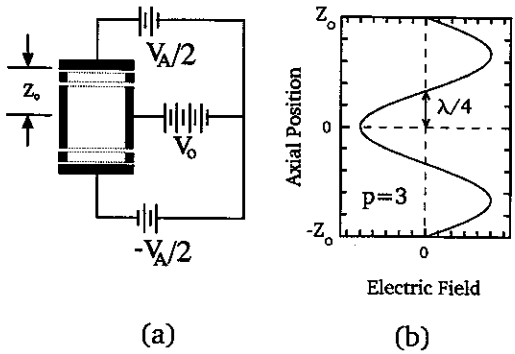

FIG. 20. (a) Antisymmetric potential across endcaps displaces electrons along the z axis. (b) Representation of transverse electric field component near the z axis for a $p = 3$ mode.

potential V_A across the endcaps (Fig. 20a). Figure 20(b) represents the magnitude of a component of the transverse electric field of a TE_{1n3} mode along the z axis. If an electron is displaced from the center of the trap (where its coupling with the cavity mode is strongest) along the z axis by a quarter wavelength to the nearest node, then its interaction with the standing wave is switched off.

Electronic control of the electron–cavity coupling is demonstrated in Fig. 21. The peak in Fig. 21(a) is due to coupling of TE_{027} to an electron cloud near the trap center. TE_{027} has 7 antinodes between the endcaps, with $\lambda/4 = 550\ \mu$m. For Fig. 21(b), the electron cloud is displaced by

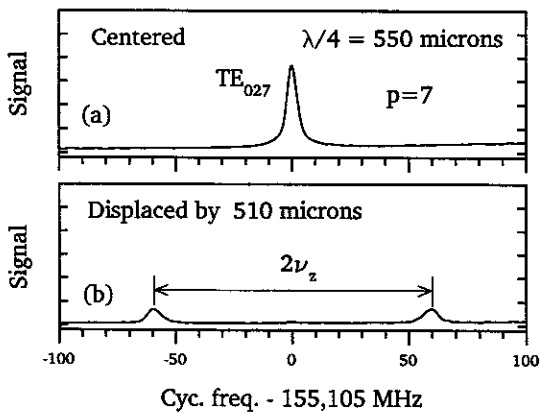

FIG. 21. (a) Observed resonance for TE_{027} ($\lambda/4 = 550\ \mu$m) with a centered electron cloud. (b) Motional doublet observed when the electrons are displaced from the center by $\Delta z = 510\ \mu$m.

510 μm from the trap center along its axis. Proximity to the node causes the resonant peak in Fig. 21(a) to disappear. Instead, a pair of peaks separated by $2\omega_z$ appear in the spectrum because the electrons are oscillating at frequency ω_z through the node at $z = \lambda/4$.

C. Sideband Cooling of Axial Motion

The axial motion of a trapped electron is dissipated as Joule heating of a resistor connected between appropriate electrodes, cooling the axial motion into thermal equilibrium with the resistor. Even at 4 K, thermal axial motions are highly undesirable in efforts to study the relativistic, quantum structure of the cyclotron oscillator, because the thermal energy is coupled into the cyclotron motion via several mechanisms.

To bring the axial motion to a much lower temperature, the electron would be decoupled from the resistor, and a sideband cooling technique (Wineland and Dehmelt, 1975; Brown and Gabrielse, 1986) would be employed. Modes with even p and $m = 1$ (e.g., in Fig. 19), when driven at $\nu_c' - \nu_z$, produce the proper oscillatory spatial gradients required to transfer the axial energy into the cyclotron motion. The cyclotron excitation in turn dissipates the transferred thermal energy into the cavity via modes with odd p and $m = 1$. It should be possible to cool the undamped axial motion to an extremely low temperature limit (Brown and Gabrielse, 1986).

$$T_z = (\nu_z/\nu_c')T_c. \tag{20}$$

With the frequencies used here, this would be an unprecedented (and extremely useful) axial temperature of 2 mK for $T_c = 4.2$ K. Because the field intensity builds up within the high Q cavity, much less drive power should be required that was estimated for propagating plane waves (Brown and Gabrielse, 1986). These same modes have a transverse magnetic field at the cavity center and could thus be used to directly flip an electron spin (when driven at ω_s). Off-resonance cyclotron excitations by the strong spin flip drive are suppressed, because these modes do not couple directly to the cyclotron motion.

IV. Electron–Cavity Interactions

The dynamics of one cyclotron oscillator localized in the midplane (near the center) of a cylindrical, microwave cavity is governed by

$$m\dot{\mathbf{v}} - (e/c)\mathbf{B} \times \mathbf{v} = e\mathbf{E}^T, \tag{21}$$

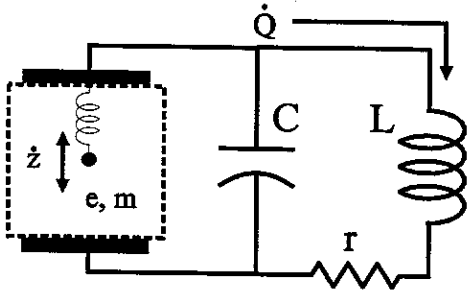

FIG. 22. Electromechanical model of electron–cavity interaction.

where $\mathbf{v} = \dot{\rho}$ is the velocity in the midplane. The transverse electric field $\mathbf{E}^T$, in the dipole approximation, is due to radiation standing-wave modes with $m = 1$ (i.e., TE_{1np} and TM_{1np}), generated as the accelerating electron radiates into the cavity. Thus, Eq. (21) indicates that the cavity standing waves act back upon the cyclotron oscillator. The calculations are classical, since it has been shown that within a high level of accuracy the exact apparatus of quantum electrodynamics yields the classical results (Boulware and Brown, 1985).

The essential features of this interaction are also contained in a simpler electromechanical model (Fig. 22) appropriate when one cavity mode is considered.[6] In this model, the selected Mth cavity mode is represented by a series LCr tuned circuit. Such a tank circuit is resonant at angular frequency $\omega_M = (LC)^{-1/2}$ with damping width $\Gamma_M = r/L$. The electron oscillator is represented as a charge e and mass m on a spring with spring constant $m(\omega_c')^2$. The electron oscillation $z(t)$ excites a current $\dot{Q}(t)$ in the tuned circuit. The oscillating current in the tuned circuit, in turn, produces an RF electric field that acts back on the electron. The interaction potential for these two coupled oscillators is given by

$$V_{\text{int}} = -\left[\frac{\kappa q}{2z_0 C}\right] z(t) Q(t), \tag{22}$$

where the dimensionless coupling $\kappa = 1$ for a capacitor with infinite parallel plates (separated by $2z_0$). Using familiar Lagrangian equations, we find that, analogous to Eq. (21),

$$m\left[\frac{d^2}{dt^2} + (\omega_c')^2\right] z(t) = -\left[\frac{\kappa q}{2z_0 C}\right] Q(t). \tag{23}$$

The excitation of the tuned circuit is described by

$$L\left[\frac{d^2}{dt^2}+\Gamma_M\frac{d}{dt}+(\omega_M)^2\right]Q(t)=-\left[\frac{\kappa q}{2z_0C}\right]z(t). \tag{24}$$

We can neglect Johnson noise (which represents the 4 K radiation of the cavity in thermal contact with the liquid helium bath).

In the weak-coupling regime (wherein the cavity field decays due to wall losses in a time shorter than required for the electron to reabsorb the radiation), the tuned circuit effectively damps the electron oscillation $z(t)$ at rate γ and shifts its resonant frequency to $\tilde{\omega}_c'$. Since the cavity modes typically have high quality factors ($Q\sim 10^3$ or higher), the damping and frequency shift take the simple forms

$$\gamma=\gamma_0\frac{1}{1+\delta^2}, \tag{25}$$

$$\tilde{\omega}_c'-\omega_c'=\frac{1}{2}\gamma_0\frac{\delta}{1+\delta^2}. \tag{26}$$

In terms of the effective resistance $R=L/(rC)$, the maximum damping rate γ_0 is given by

$$\gamma_0=\left[\frac{\kappa q}{2z_0}\right]\frac{R}{m}. \tag{27}$$

The resonant frequencies of the tuned circuit and electron motion are ω_M and ω_c, respectively, when the interaction is turned off. The unperturbed resonance frequency of the two oscillators are related by a detuning δ defined by

$$\omega_c'=\omega_M+\tfrac{1}{2}\Gamma_M\delta. \tag{28}$$

If the electron oscillator and the LCr circuit are tuned to the same unperturbed resonance frequency (i.e., $\delta=0$), there is no frequency shift, but the dampling rate is at its maximum. When $\delta\neq 0$, the dampling rate is reduced, but the resonant frequency of the electron oscillator is shifted. The maximum frequency shifts $\pm\gamma_0/4$ occur near resonance, at detunings $\delta=\pm 1$. The characteristic shapes for γ and $\Delta\omega$ are shown in Fig. 5 and are clearly evident in more detailed calculations.

Since $\gamma_0\sim R\sim Q_M$, the maximum damping and maximum frequency shift are larger when the quality factor $Q_M=\omega_M/\Gamma_M$ is larger. To display the Q dependence explicitly, we write

$$\frac{\gamma_0}{\omega_M}=2Q_M\left(\frac{\lambda_M}{\omega_M}\right)^2, \tag{29}$$

thereby defining the coupling strength λ_M.[7] This definition also allows the use of a simple form for the electron's frequency shift and damping rate,

$$\Delta\omega - i\frac{\gamma}{2} = \frac{\omega(\lambda_M)^2}{\omega^2 + i\omega\Gamma_M - \omega_M^2}, \tag{30}$$

which can be generalized to include interactions with more than one cavity mode by summing the right-hand side over the mode index M.

For Eq. (30) and its generalization to be quantitatively useful, the coupling constants $\lambda_M^2 = \lambda_{n,l}^2$ have been calculated for regular cavities of interest (Gabrielse *et al.*, 1990). In particular, for the cylindrical cavity, the mode index M is identified here with the two quantum number $n = 0, 1, 2, \ldots$ and $l = 1, 2, 3, \ldots$. When the magnetic field is along the symmetry axis of the cavity, these two indices identify the subset of cavity modes that couple to a cyclotron oscillator located at the center of the cavity. Two types of modes couple to the cyclotron motion, and for both it is convenient to use $k_n = (n + 1/2)\pi/z_0$. For TE (transverse electric) modes,

$$\lambda_{n,l}^2 = \frac{r_e c^2}{z_0 \rho_0^2} \frac{2}{\alpha_l^2 - 1} \frac{\alpha_l^2}{J_1(\alpha_l)^2}, \tag{31}$$

$$\omega_{n,l}^2 = \left(k_n^2 + \frac{\alpha_l^2}{\rho_0^2}\right)c^2, \tag{32}$$

where α_l (defined by $J_1'(\alpha_l) = 0$) is the lth zero of the derivative of the first order Bessel function. For TM (transverse magnetic) modes that couple to electron cyclotron motion,

$$\lambda_{n,l}^2 = \frac{r_e c^2}{z_0 \rho_0^2} \frac{2k_n^2 c^2}{\omega_{n,l}^2} \frac{1}{J_0(\beta_l)}, \tag{33}$$

$$\omega_{n,l}^2 = \left(k_n^2 + \frac{\beta_l^2}{\rho_0^2}\right)c^2, \tag{34}$$

where β_l (given by $J_1(\beta_l) = 0$) is the lth zero of the first order Bessel function. The quantum numbers n and l that we use to label the cavity modes that couple to the electron are simply related to common conventions for labeling all the modes of a cylindrical cavity. For example, in the textbook by Jackson (1975) the origin of the coordinate system is translated to the center of the bottom endcap, and the TE and TM modes identified in the foregoing are labeled as $TE_{1,l,2n+1}$ and the

$TM_{1,l,2n+1}$, respectively. Couplings for other cavity geometries of interest are found in an earlier work (Gabrielse *et al.*, 1990).

Unfortunately, the simple theory is afflicted with problems arising from the self-field interaction. To see this, we note that the standing-wave field is actually composed of two contributions

$$\mathbf{E}^{\mathrm{T}} = \mathbf{E}_{\mathrm{self}} + \mathbf{E}', \tag{35}$$

the self-field $\mathbf{E}_{\mathrm{self}}$ radiated directly by the oscillator (as if into free space) and the reflected field $\mathbf{E}'$, which is reflected from the cavity walls. The back reaction of a self-field upon the accelerating charge that is radiating is well known to lead to difficulties and divergences in classical electricity and magnetism[8] (inherited by QED in addition to divergences of its own). In our particular situation, the real part of the mode sum

$$\Delta\omega - i\frac{\gamma}{2} = \omega - \omega_{\mathrm{c}} - i\frac{\gamma_{\mathrm{c}}}{2} = \omega \sum_{M} \frac{\lambda_M^2}{\omega^2 + i\omega\Gamma_M - \omega_M^2} \tag{36}$$

diverges when the sum includes all the cavity modes. For a correctly renormalized calculation, the self-field term is replaced by a radiation damping term for radiation into free space (with damping rate γ_{c}) and only the transverse reflected field $\mathbf{E}'$ acts back upon the cyclotron oscillator, so that Eq. (21) is rewritten as

$$\dot{\mathbf{v}} - \omega_{\mathrm{c}} \times \mathbf{v} + (\gamma_{\mathrm{c}}/2)\mathbf{v} = (e/m)\mathbf{E}'. \tag{37}$$

Only in special cases is it possible to separate the reflected field and the self-field that together make up the standing wave. The high degree of symmetry for a spherical cavity (Brown *et al.*, 1986; Dehmelt, 1984) makes the removal of the self-field relatively simple because the free-space radiation from the oscillator at the center contains only outgoing spherical waves, easily distinguished from the reflected waves. A cylindrical cavity (Brown *et al.*, 1985a,b) has less symmetry, but the separation can still be accomplished by using image charges to satisfy the cavity boundary conditions. The reflected field is thus clearly distinguished as the field of the images. For a hyperbolic cavity (which corresponds to the trap within which the electron's magnetic moment was measured) a separation of self and reflected fields is completely intractable. Finite mode sums as done in the simple model are the only possibility. Conditions of a modified mode sum and a complete calculation for the cylindrical cavity are used to estimate the optimal number of terms to be included in the finite mode sum, even though the mode density is significantly higher in a hyperbolic cavity.

The usefulness of the simple theory is limited especially when the

electron cyclotron oscillator is not near to resonance with a high Q cavity mode. A detailed discussion of how the divergences arise and can be partially circumvented in this model has been presented (Brown *et al.*, 1988; Gabrielse *et al.*, 1990). In general, the contribution from any off-resonant (Mth) mode to the frequency shift $\Delta\omega$ of the electron oscillator, going as $\frac{1}{2}(\lambda_M)^2/(\omega_c - \omega_M)$ (independent of Q_M), is overstated slightly due to self-field in the standing wave. The overstated contributions add up as the contributions from many modes are included. Optimal use of the simple mode sum model thus requires a careful choice of the number of cavity modes included in the sum. Beyond a certain number of terms, the real part of the mode sum will start to diverge. Eventually, the mode sum over an infinite number of such small contributions diverges. It is difficult to establish the optimum number of terms of the accuracy of the truncated mode sum except by comparision with a calculation that avoids the divergences entirely (Brown, *et al.*, 1988). A modified mode sum formula was obtained (Brown *et al.*, 1988), which converges for the case of a cylindrical cavity and can be used to obtain the unshifted cyclotron frequency to 1 part in 10^9.

V. Summary and Future

The most accurate tests of quantum electrodynamics have been seriously interrupted by modifications to the QED vacuum by the cavity formed by the metal electrodes of a Penning trap. A new cylindrical Penning trap cavity has standing-wave radiation modes that can be classified in a familiar way and described by simple analytic expressions. Geometric tricks make it possible to suspend and study a single electron localized in this cavity. A new technique, utilizing the coherent response of trapped electrons that are parametrically pumped, makes it possible to measure resonant frequencies and quality factors for more than 100 radiation modes, in situ at 4 K. In addition to the interesting studies of the nonlinear dynamics of the cooperative electron motions that have been initiated, this is the first time that the radiation field in a trap cavity has been understood. The electron–cavity interaction is understood well enough to offer the possibility of cooling an electron's motion to subtantially lower temperatures, for example, and of avoiding the cavity shifts of measured electron frequencies that have been plaguing measurements of the electron's magnetic moment. A new generation of tests of QED can now be undertaken that are not limited by either radiation damping width or by cavity shifts.

Acknowledgments

We are grateful to C. H. Tseng for experimental support. This work was supported by the National Science Foundation and the Office of Naval Research.

Notes

1. The most recent and accurate calculation is in Kinoshita, 1990.
2. We will use frequency ν or angular frequency $\omega = 2\pi\nu$ depending on which is more convenient.
3. Cavity-like effects were observed earlier with fatty acid molecules near the surface of a conducting plate (Drexhage, 1974).
4. Reviewed in Haroche and Kleppner, 1989.
5. Reviewed in Hinds, 1990.
6. It is customary in microwave electronics to present information in the form of equivalent circuits. See, for example, Beringer, 1948.
7. This is the definition of $(\lambda_M)^2$ used in Brown *et al.*, 1985b. It is smaller than the dimensionless $(\lambda_M)^2$ used in Brown *et al.*, 1988, by a factor of $\omega_M^2 r_e / z_0$.
8. See, for example, Panofsky and Phillips, 1962; also Chapter 17 of Jackson, 1975.

References

Barut, A. O., and Dowling, J. P. (1989). *Phys. Rev. A* **39,** 2796.
Beringer, R. (1948). In *Principles of Microwave Circuits,* C. G. Montgomery, R. H. Dicke, and E. M. Purcell, eds., MIT Rad. Lab. Series 8, McGraw, New York, p. 207.
Boulware, D. G., and Brown, L. S. (1985). *Phys. Rev. Lett.* **55,** 133.
Boulware, D. G., Brown, L. S., and Lee, T. (1985). *Phys. Rev. D* **32,** 729.
Brown, L. S., and Gabrielse, G. (1986). *Rev. Mod. Phys.* **58,** 233.
Brown, L. S., Gabrielse, G., Helmerson, K., and Tan, J. (1985a). *Phys. Rev. Lett.* **55,** 44.
Brown, L. S., Gabrielse, G., Helmerson, K., and Tan, J. (1985b). *Phys. Rev. A* **32,** 3204.
Brown, L. S., Helmerson, K., and Tan, J. (1986). *Phys. Rev. A* **34,** 2638.
Brown, L. S., Gabrielse, G., Tan, J., and Chan, K. C. D. (1988). *Phys. Rev. A* **37,** 4163.
Conti, R., Newman, D., Rich, A., and Sweetman, E. (1984). In *Precision Measurements and Fundamental Constants II,* B. N. Taylor and W. D. Phillips, eds., Spec. Publ. 617, U.S. National Bureau of Standards, p. 207.
Dehmelt, H. G. (1984). *Proc. Natl. Acad. Sci. U.S.A.* **81,** 8037; Erratum, *ibid.* **82,** 6366 (1985).
Drexhage, K. H. (1974). In *Progress in Optics,* Vol. 12, E. Wolf, ed., Elsevier Science Publishers B. V., Amsterdam, p. 165.
Fishbach, E., and Nakagawa, N. (1984a). *Phys. Lett.* **149B,** 504.
Fishbach, E., and Nakagawa, N. (1984b). *Phys. Rev. D* **30,** 2356.
Gabrielse, G., and Dehmelt, H. G. (1985). *Phys. Rev. Lett.* **55,** 67.

Gabrielse, G., and MacKintosh, F. C. (1984). *Int. J. Mass Spectrom. Ion Process* **57,** 1.
Gabrielse, G., Dehmelt, H., and Kells, W. (1985). *Phys. Rev. Lett.* **54,** 537.
Gabrielse, G., Tan, J., and Brown, L. S. (1990). In *Quantum Electrodynamics,* T. Kinoshita, ed., World Scientific, Singapore, p. 389.
Haroche, S., and Kleppner, D. (1989). *Physics Today* (January), p. 24.
Hinds, E. A. (1990). *Adv. Atom. Mol. Opt. Phys.* **28,** 231.
Hulet, R. G., Hilfer, E. S., and Kleppner, D. (1985). *Phys. Rev. Lett.* **55,** 2137.
Jackson, J. D. (1975). *Classical Electrodynamics,* 2nd ed., Wiley, New York.
Kasevich, M., and Chu, S. (1991). *Phys. Rev. Lett.* **67,** 181.
Kinoshita, T. (ed.) (1990a). *Quantum Electrodynamics,* World Scientific, Singapore.
Kleppner, D. (1971). In *Atomic Physics and Astrophysics,* M. Chrétien and E. Lipworth, eds., Gordon and Breach, New York, p. 5.
Kleppner, D. (1981). *Phys. Rev. Lett.* **47,** 233.
Kreuzer, M. (1988). *J. Phys. A* **21,** 3285.
Kreuzer, M., and Svozil, K. (1986). *Phys. Rev. D* **34,** 1429.
Panofsky, W. K. H., and Phillips, M. (1962). *Classical Electricity ad Magnetism,* 2nd ed., Addison-Wesley, Reading, Mass., Chapters 21 and 22.
Purcell, E. M. (1946). *Phys. Rev.* **69,** 681.
Svozil, K. (1985). *Phys. Rev. Lett.* **54,** 742.
Tan, J., and Gabrielse, G. (1989). *Appl. Phys. Lett.* **55,** 2144.
Tan, J., and Gabrielse, G. (1991). *Phys. Rev. Lett.* **67,** 3090.
Tan, J., and Gabrielse, G. (1993). *Phys. Rev. A,* (in press).
Tang, A. C. (1987). *Phys. Rev. D* **36,** 2181.
Taylor, B. N. (1991). Private communication.
Van Dyck, R. S., Jr. (1990). In *Quantum Electrodynamics,* T. Kinoshita, ed., World Scientific, Singapore, p. 322.
Van Dyck, R. S., Jr., Moore, F. L., Farnham, D. L., Schwinberg, P. B., and Dehmelt, H. G. (1987a). *Phys. Rev. A* **36,** 3455.
Van Dyck, R. S., Jr., Schwinberg, P. B., and Dehmelt, H. G. (1987b). *Phys. Rev. Lett.* **59,** 26.
Wineland, D., and Dehmelt, H. (1975). *Int. J. Mass Spectrom. Ion Phys.* **16,** 338; Erratum, *ibid.,* **19,** 251 (1975).